ISSN: 2455 – 9938
PubMed- National Library of Medicine - ID: 101731611

EIJO: Journal of Science, Technology and Innovative Research (EIJO–JSTIR)
Einstein International Journal Organization (EIJO)
Available Online at:www.eijo.in
Volume – 11, Issue – 1, January – February - 2026, Page No. : 01 - 14

Advanced Structural and Microstructural Metrology of Semiconductor Nanocrystals via Rietveld Refinement: A Systematic Review

[1]Ramesh Chand Meena, Research Scholar, Faculty of Education and Methodology, Jayoti Vidyapeeth Women's University Jaipur Rajasthan.

[2]Nayan Mishra, Associate Professor, Faculty of Education and Methodology, Jayoti Vidyapeeth Women's University Jaipur Rajasthan.

Corresponding Author: Nayan Mishra, Associate Professor, Faculty of Education and Methodology, Jayoti Vidyapeeth Women's University Jaipur Rajasthan.

Type of Publication: Original Research Article

Conflicts of Interest: Nil

Abstract

The transition from bulk semiconductors to nanocrystalline regimes introduces profound structural complexities, including lattice expansion, symmetry breaking, and significant microstrain. Traditional peak-profile analysis often fails to decouple these intrinsic material properties from instrumental artifacts. This review critically evaluates the Rietveld refinement method as a holistic approach for the structural characterization of semiconductor nanocrystals (NCs). We provide a rigorous mathematical treatment of the whole-powder-pattern-fitting (WPPF) algorithm, focusing on the convolution of Lorentzian and Gaussian functions to model size and strain effects. Furthermore, we examine the influence of cation distribution, vacancy ordering, and stacking faults in diverse systems including II-VI, III-V, and the emerging metal-halide perovskites. By synthesizing recent advancements in software capabilities and synchrotron-based high-resolution diffraction, this article serves as a definitive guide for achieving sub-angstrom structural precision in nanomaterials research.

Keywords: Rietveld Refinement, Semiconductor Nanocrystals, Microstrain, Diffraction Modeling, Structural Metrology.

1. Introduction

The Paradigm Shift in Nanoscale Characterization

The relentless pursuit of Moore's Law and the advent of "More-than-Moore" technologies have necessitated the synthesis of semiconductor nanocrystals with atomic-level precision. At the nanoscale, the high surface-to-volume ratio leads to a significant percentage of atoms residing in a non-equilibrium environment, resulting in lattice relaxation or contraction. Conventional X-ray diffraction (XRD) interpretation, primarily based on the Scherrer equation, provides only a rudimentary estimation of the "apparent" crystallite size and ignores the vital contribution of lattice strain and instrumental broadening (Sinha et al., 2025).

Rietveld refinement transcends these limitations by employing a least-squares minimization protocol that fits the entire diffraction profile based on a calculated crystallographic model. For semiconductor NCs, this allows for the simultaneous refinement of unit cell parameters, atomic coordinates, isotropic/anisotropic displacement parameters ($B_{\{iso\}}$), and phase

fractions. The complexity of semiconductor NCs often manifesting as core-shell architectures or doped matrices demands a characterization tool that can differentiate between chemical substitution and physical defect density. Consequently, Rietveld analysis has transitioned from a purely structural tool to a microstructural diagnostic, capable of correlating lattice distortion with optoelectronic performance (Lee & Xu, 2020; Patra et al., 2009). As semiconductor technologies transition toward sub-5 nm regimes, the demand for precise structural characterization has reached a critical juncture. The Rietveld method, once reserved for bulk polycrystalline powders, has evolved into a sophisticated diagnostic for nanocrystalline materials. This review provides a comprehensive synthesis of the Rietveld refinement process applied to semiconductor nanocrystals (NCs), moving beyond the simplistic Scherrer approximations. We examine the mathematical convolution of instrumental and specimen-induced broadening, the modeling of anisotropic crystallite shapes using spherical harmonics, and the quantification of lattice strain. Furthermore, we discuss the integration of high-resolution synchrotron data and the emerging role of Machine Learning (ML) in automating parameter optimization.

This article aims to provide a rigorous framework for researchers to achieve sub-picometer structural resolution, facilitating the rational design of next-generation optoelectronic devices. The characterization of semiconductor nanocrystals (NCs) has historically relied on a combination of transmission electron microscopy (TEM) and rudimentary X-ray diffraction (XRD) analysis. However, as the "quantum size effect" becomes the dominant driver of optical and electronic properties, the need for a more holistic structural probe has become apparent. TEM, while providing direct visualization, often suffers from poor statistical sampling and beam-induced damage, particularly in sensitive metal-halide perovskites or chalcogenides. Conversely, powder XRD provides a bulk-averaged perspective but is frequently misinterpreted using the Scherrer equation, which fails to account for microstrain, lattice gradients, and instrumental aberrations (Sinha et al., 2025).

The Rietveld method represents a paradigm shift from "peak-fitting" to "structure-refining." By calculating the entire diffraction profile from first principles including the space group symmetry, atomic positions, and thermal displacement parameters the Rietveld approach allows for the decoupling of multiple physical phenomena that overlap in the $2\theta_i$ domain. In the contemporary research environment of 2026, where "device-grade" nanocrystals require strict phase purity and defect control, Rietveld analysis serves as the primary tool for verifying cation distribution and lattice relaxation. This introduction explores the transition from the kinematic scattering limit to the complex, non-equilibrium structures found in colloidal quantum dots and mechanosynthesized nanopowders (Lee & Xu, 2020; Patra et al., 2009)

2. Theoretical Foundations and Profile Modeling

2.1 The Mathematics of Whole-Pattern Fitting

The Rietveld method operates on the principle of minimizing the residual variance between the experimental observation and a theoretical model derived from the Space Group symmetry. The total calculated intensity at any given point $2\theta_i$ is a summation of the background, the peaks from multiple phases, and the noise components. The structure factor F_k, which carries the information of the atomic arrangement within the unit cell, is defined as:

$$F_k = \sum_j N_j f_j \exp[2\pi i(hx_j + ky_j + lz_j)] \exp[-M_j]$$

In the Reitveld refinement the total diffracted intensity Y_{ci} from a powder mixture of several phases corresponding to the angular position $2\theta_i$ of the pattern, is calculated using the following equation:

$$Y_{ci} = S\sum_k L|F_k|^2 \Phi(2\theta_i - 2\theta_k)P_k A + Y_{bi}$$

where S is the scale factor

K represents the miller indices h, k, l for a Bragg reflection

L_k contains the Lorentz's polarization and multiplicity factors.

F_k is the structure factor for k^{th} Bragg reflection

□ is the reflection profile function

P_k is a preferred orientation function

A is the absorption factor it differs with instrument geometry. It is usually taken to be a constant for the instrument geometry used for X-ray diffractometers.

Y_{bi} is the background intensity at i^{th} step

$$Y_{bi} = \sum_k B_m[(2\theta_i(BKPOS) - 1)]^m$$

where BKPOS is a user specified value. This function is designed to account for background contributions from an amorphous or nanocrystalline phase.

The least squares refinements were carried out until the best fit was obtained, between the entire observed powder diffraction taken as a whole and the entire calculated pattern based on the simultaneously refined models, for the crystal structure, diffraction optics effects, instrumental factors and other specimen characteristics (e.g lattice parameter, space group). The best fit sought was the best least squares fit to all of the thousands of $Y_{i's}$ simultaneously. The quantity minimized in the least squares refinement is the residual S_y

$$S_y = \sum_i W_i(y_i - y_{ci})_2$$

where $W_i=1/y_i$

Y_i=observed intensity at the i^{th} step

Y_{ci}=calculated intensity at the i^{th} step and the sum is the overall data points.

The profile functions used to describe the diffraction peaks, so determined in the fitting procedure, were used to obtain the microstructural parameters: crystallite size and microstrain. In this way an accurate quantitative determination of the weight fractions of the different phases occurring in the sample as well as their structural and microstructural features could be discussed.

The peak position 2θ & the peak width in the observed profiles depend on several factors such as particle size, imperfection etc. The imperfections include the dimensions and morphology of coherently diffracting domains, variation in interatomic distances due to internal stress or non-stoichoimetry, stacking faults, micro-twinning, dislocations and other forms of atomic disorder. Micro structural features directly influence the shape of line profiles which influence direction

and magnitude of the diffraction vector. Therefore, line-shape parameter doesn't vary smoothly with 2θ or d. However, in the absence of imperfection broadening, the full width at half maximum can be modeled as

$$H = Uta\, n^2\theta + V \tan\theta + W$$

where H has been taken on 2θ scale

Here, U, V, W are Caglioti parameters representing instrumental effects, while X and Y are refined to extract microstrain and crystallite size, respectively (Lee & Xu, 2020; Sinha et al., 2025).

In the presence of imperfection broadening such a smooth variation is isotropic (independent of lattice direction). Thompson et. al (1987) developed a procedure based on imposed isotropy. The authors used a special pseudo voigt function, which is the linear combination of Lorentzian and Gaussian functions given as

$$P(t) = \eta L(t,\tau) + (1-\eta)G(t,F)$$

where $G(t,F)$ is the Gaussian function given as

$$G(t,F) = \frac{1}{\sqrt{2\Lambda H^2}} e^{-\frac{(\tau-t)^2}{2H^2}}$$

where H^2 is the coefficient for Gaussian variance

Γ used is simply a symbol related to the profile breadth.

And $L(t,\tau)$ is the Lorentzian function

$$L(t,F) = \frac{\tau}{2\pi}\left[\frac{1}{\left(\frac{\tau}{2}\right)^2 + t^2}\right]$$

η is the mixing factor given by Thompson (1987)

2.2 Background and Convergence Criteria

A significant challenge in nanocrystal refinement is the presence of a "diffuse" background, often caused by surface amorphous layers or solvent scattering in colloidal samples. Advanced refinements utilize Chebyshev polynomials or real-space background modeling to prevent the absorption of Bragg intensity into the background function. The convergence of the refinement is statistically validated through the Weighted Profile R-factor (R_{wp}) and the Goodness of Fit (\chi^2). For a Q1-level publication, a \chi^2 value between 1.0 and 1.5 is generally required to prove that the model accounts for all physical phenomena within the sample (Kumar et al., 2013).

2.3 Convolution and Shape Functions

At the heart of any high-impact Rietveld refinement is the Profile Shape Function (PSF). In anocrystals, the diffraction peak is a convolution of the instrumental response and the sample's intrinsic broadening. The Thompson-Cox-Hastings (TCH) pseudo-Voigt function is currently the gold standard, as it treats the Gaussian (G) and Lorentzian (L) components independently. For semiconductors, the Gaussian component (H_G) typically models the instrumental effects and the strain distribution, while the Lorentzian component (H_L) captures the size-induced broadening.

Mathematically, the peak width is defined by the Caglioti formula, where U, V, and W parameters must be meticulously refined using a standard reference material (e.g., NIST Si 640f). In nanocrystalline regimes, the Y parameter (Lorentzian size broadening) becomes dominant, often following a 1/\cos \theta relationship. However, a common pitfall in lower-tier research is the neglect of the X parameter (Lorentzian strain), which can lead to significant errors in crystallite size estimation. Advanced refinements in 2026 now incorporate the Popa model for anisotropic broadening, allowing for the determination of crystallite morphology (e.g., nanoplatelets vs. nanowires) directly from the diffraction pattern (Sinha et al., 2025; Thompson et al., 2026).

2.4 The Background and Scattering Physics

The background in nanocrystal XRD is rarely a simple linear function. It consists of incoherent scattering, thermal diffuse scattering (TDS), and contributions from the sample holder or solvent. In Scopus Q1-level research, modeling the background with high-order Chebyshev polynomials (typically 12th to 20th order) is essential to ensure that the intensity at the "tails" of the broadened peaks is correctly attributed. Furthermore, for quantum dots with high surface-disorder, a "Bragg-Brentano" geometry may introduce significant air scattering, necessitating the use of vacuum chambers or specific background subtraction protocols. The integration of the Pair Distribution Function (PDF**)** into the Rietveld workflow has recently emerged as a method to account for the amorphous surface shell, providing a "Total Scattering" solution that captures both long-range order and local distortions (Lee & Xu, 2020).

3. Microstructural Decoupling: Size, Strain, and Defects

3.1 The Physical Significance of Microstrain

In semiconductor NCs, microstrain (\epsilon) is not merely a statistical error but a physical representation of lattice defects, such as dislocations and vacancies. In systems like ZnO and GaN, nitrogen or oxygen vacancies induce a non-uniform distribution of d-spacings, leading to a Lorentzian broadening that increases with \tan \theta. Rietveld refinement allows for the separation of this strain from the size-induced broadening, which follows a 1/\cos \theta dependence. By applying a Phenomenological Size-Strain model, researchers can map the distribution of strain across different crystallographic directions (anisotropy). For instance, in 1D nanostructures like CdSe nanorods, the broadening of the (002) reflection is significantly narrower than the (100) and (110) reflections, a phenomenon that can only be accurately modeled using spherical harmonics or the Popa model within the Rietveld framework (Patra et al., 2009; Sinha et al., 2025).

In semiconductor NCs, the lattice constant is not a static value but a function of the particle size. This "lattice contraction" or "expansion" is often driven by surface tension and the presence of capping ligands. Rietveld refinement allows for the determination of the hydrostatic strain, which is the uniform change in the unit cell volume, and the microstrain, which represents the root-mean-square variation in d-spacings. In systems like InP/ZnS core-shell quantum dots, the interfacial strain between the core and the shell can be refined using a multi-phase Rietveld model, where the lattice parameters of each phase are constrained by the epitaxial relationship. Current research highlights that microstrain is a primary predictor of non-radiative recombination rates in solar cells. By refining the isotropic displacement parameters (B_{iso}**)**, researchers can quantify the degree of atomic "rattling" within the lattice. A high B_{iso} value for the cation site often indicates a high density of point defects or a transition toward a glass-like state. Through rigorous refinement of the

occupancy factors (Occ), one can detect stoichiometric deviations (e.g., oxygen vacancies in ZnO) with an accuracy of \pm 1\%, a level of detail that is inaccessible via EDS or XPS alone (Gomez-Vargas et al., 2024; Kumar et al., 2013).

3.2 Stacking Faults and Planar Defects

Semiconductors with the diamond or zinc-blende structure are prone to stacking faults (e.g., the transition from cubic ABC to hexagonal ABAB stacking). These faults result in characteristic peak shifts and asymmetry that cannot be modeled by simple Voigt functions. Software like MAUD (Materials Analysis Using Diffraction) integrates the Warren-Averbach theory to refine stacking fault probabilities directly from the powder pattern. This is essential for understanding the phase stability of nanocrystalline ZnS and SiC, where the energy barrier between polytypes is minimal at the nanoscale (Patra et al., 2009). Many high-performance semiconductors, such as SiC and GaN, exhibit polytypism the existence of multiple stacking sequences of the same atomic layers. In nanocrystals, the energy difference between the cubic (zinc-blende) and hexagonal (wurtzite) phases is often negligible, leading to high concentrations of stacking faults. These faults manifest as "twinning" or "streaking" in diffraction patterns, which the Rietveld method can model using the Warren-Averbach approach. Sophisticated software like MAUD now allows for the refinement of the "faulting probability," providing a quantitative measure of how often the stacking sequence is interrupted. This is critical for 2D semiconductors like MoS_2, where the transition from 2H to 1T phases dictates the material's catalytic activity (Patra et al., 2009; Sinha et al., 2025).

4. Analytical Software and Computational Strategies

4.1 Comparison of Algorithmic Implementations: From Le Bail to Pythonic Frameworks

The evolution of Rietveld software has moved from rigid, command-line interfaces to modular, extensible ecosystems capable of handling multi-dimensional datasets. GSAS-II represents a significant leap forward, utilizing a Python-based core that allows for the seamless integration of custom scripts for batch processing. This is particularly vital in the study of semiconductor NCs, where a single synthesis run may produce dozens of samples with varying doping concentrations. GSAS-II’s ability to perform sequential refinements where the results of one refinement serve as the starting model for the next ensures consistency across a series of structural evolutions (Lee & Xu, 2020).

Software	Core Strength	Key Application for Semiconductors
FullProf	Highly versatile, strong for magnetic structures.	Doped oxides (e.g., ZnO, TiO _2) (Engineered Science Publisher, n.d.).
MAUD	Excellent for microstructure, textures, and thin films.	Quantum dots and mechanosynthesized powders (Patra et al., 2009).
GSAS-II	User-friendly, modern Python-based framework.	General structural refinement and synchrotron data (Lee & Xu, 2020).

Software	Core Strength	Key Application for Semiconductors
TOPAS	Fundamental parameters approach; commercial but powerful.	Industrial phase quantification and high-throughput analysis (Lee & Xu, 2020).

In contrast, FullProf remains unparalleled for systems where magnetism and structure are inextricably linked, such as in diluted magnetic semiconductors (DMS). Its robust implementation of the Marquardt-Levenberg algorithm for non-linear least-squares minimization provides superior convergence in cases where peak overlap is severe. For nanocrystals exhibiting significant texture or preferred orientation common in spin-coated thin films MAUD (Materials Analysis Using Diffraction) employs a "hierarchical" refinement strategy. MAUD is unique in its capacity to incorporate the Popa model for anisotropic size-strain broadening and the WIMV algorithm for texture analysis, making it the software of choice for quantifying the structural integrity of 2D TMDs and nanowires (Sinha et al., 2025).

4.2 The Role of "Fundamental Parameters" and Absolute Metrology

The Fundamental Parameters Approach (FPA**)** has revolutionized the extraction of physical data from broadened nanocrystalline profiles. Traditional methods rely on a "standard" (like LaB_6) to subtract instrumental broadening, but this assumes the standard and sample share identical optical paths. FPA, implemented in TOPAS and modern versions of BGMN, calculates the instrumental resolution function (IRF) by convolving the physical dimensions of the diffractometer such as the source emission profile, the goniometer radius, and the detector slit widths via ray-tracing protocols.

For semiconductor NCs, where the Bragg peaks are often 10–50 times broader than the instrumental contribution, FPA provides a "noise-free" baseline. This allows for the refinement of the Lorentzian crystallite size (L) and Gaussian microstrain (G) as absolute physical values. In 2026, researchers are increasingly using FPA to detect "strain gradients" within individual quantum dots, where the core and the surface layers exhibit different lattice constants. By eliminating the reliance on external standards, FPA reduces the "systematic error budget," allowing for the detection of lattice parameter shifts as small as 10^ {-4} Å (Kis et al., 2024; Thompson et al., 2026).

4.3 Emergent Computational Paradigms: AI and Bayesian Refinement

A critical bottleneck in Rietveld analysis is the "user-dependency" of the results. To mitigate this, Bayesian optimization and Genetic Algorithms (GAs) are being integrated into the refinement workflow. These AI-driven strategies explore the high-dimensional parameter space (2\theta shifts, thermal factors, occupancies) to avoid local minima that often trap manual refinements. By employing a Probabilistic Graphical Model, software can now estimate the uncertainty of refined parameters more accurately than traditional R -factors. This "Automated Rietveld" approach is essential for the rapid screening of semiconductor libraries, where the structural phase must be correlated with high-throughput photoluminescence (PL) data in real-time (arXiv, 2025; Miller & Tan, 2024).

5. Case Studies: From Wide-Bandgap Oxides to Perovskites

5.1 Doped Transition Metal Oxides: Quantifying Substitutional Dynamics

In the realm of wide-bandgap semiconductors like ZnO and TiO_2, Rietveld refinement serves as the definitive tool for distinguishing between substitutional doping and interstitial incorporation. When a transition metal like Mn or Co is

introduced into the ZnO wurtzite lattice, the refinement of the internal structural parameter (u) which defines the cation-anion distance along the c -axis reveals the degree of local tetrahedral distortion.

A critical observation in recent literature is the correlation between the **c**/a ratio and the magnetic exchange interaction. As the dopant concentration crosses a critical threshold, Rietveld analysis often detects a transition from a paramagnetic to a "cluster-glass" state, identified by a slight but statistically significant increase in the Isotropic Displacement Parameter (B_{iso}) of the oxygen site. This increase indicates a localized "rattling" of atoms due to oxygen vacancies (V_O), which are often the true mediators of ferromagnetism in DMS systems (CORE, n.d.; Engineered Science Publisher, n.d.).

5.2 Metal-Halide Perovskite Quantum Dots: Octahedral Tilting and Stability

The structural volatility of APbX_3 perovskites necessitates a rigorous whole-pattern approach. While these materials often appear "cubic" in low-resolution XRD, Rietveld refinement of high-resolution data frequently uncovers lower-symmetry tetragonal (P4/mmm) or orthorhombic (Pnma) phases. The key to these refinements is the Glazer notation for octahedral tilting. By refining the Pb-X-Pb bond angles, researchers can quantify the "chemical pressure" exerted by the A -site cation (e.g., Cs^+ vs. CH_3NH_3^+).

Recent breakthroughs in 2025 have shown that surface-ligand engineering can "lock" the high-symmetry cubic phase of CsPbI3, which is otherwise unstable at room temperature. Rietveld analysis of these ligand-stabilized NCs reveals a non-uniform compressive strain that originates at the surface and penetrates ~2 nm into the core. This strain effectively "stiffens" the lattice, reducing the electron-phonon coupling and resulting in the ultra-narrow emission linewidths required for next-generation displays (World Scientific Publishing, 2024; Zhao & Wang, 2025).

5.3 Complex Chalcogenides and Core-Shell Architectures

Beyond binary systems, Rietveld refinement is now being applied to ternary and quaternary chalcogenides (e.g., $CuInS_2$, CZTS). In these materials, cation disorder (the random swapping of Cu and Zn sites) is a major cause of voltage loss in solar cells. By refining the Site Occupancy Factors (SOF) using anomalous X-ray scattering data, Rietveld models can quantify the "degree of kesterite-stannite ordering."

Furthermore, for core-shell heterostructures (e.g., CdSe/ZnS), the refinement must account for the epitaxial mismatch. A dual-phase Rietveld model is typically employed, where the lattice parameters of the shell are constrained by the core dimensions. The resulting interfacial strain refined from the peak asymmetry is directly correlated with the stability of the quantum dot against photo-oxidation. This level of structural "dissection" ensures that the synthesized NCs meet the stringent requirements of Q1-level materials engineering (Zhang et al., 2025; Gomez-Vargas et al., 2024). The structural integrity of core–shell nanostructures is the primary determinant of their exciton dynamics and photoluminescence stability. In the comparative study of conventional (CdSe/ZnS) and inverted (ZnS/CdSe) nanostructures by Optical and Quantum Electronics (2018), Rietveld refinement served as the critical diagnostic tool to resolve the complex interplay between phase evolution and interfacial strain.For both conventional and inverted architectures, the diffraction profiles were modeled using the Whole Powder Pattern Fitting (WPPF) approach. The primary challenge in these systems is the significant lattice mismatch approximately 12% between the CdSe (a \approx 6.05 Å) and ZnS (a \approx 5.41 Å) cubic zinc-blende phases (Space Group: F\bar {4}3m). Rietveld refinement allowed researchers to differentiate between a truly epitaxial core–shell growth and a simple physical mixture of independent nanocrystals.

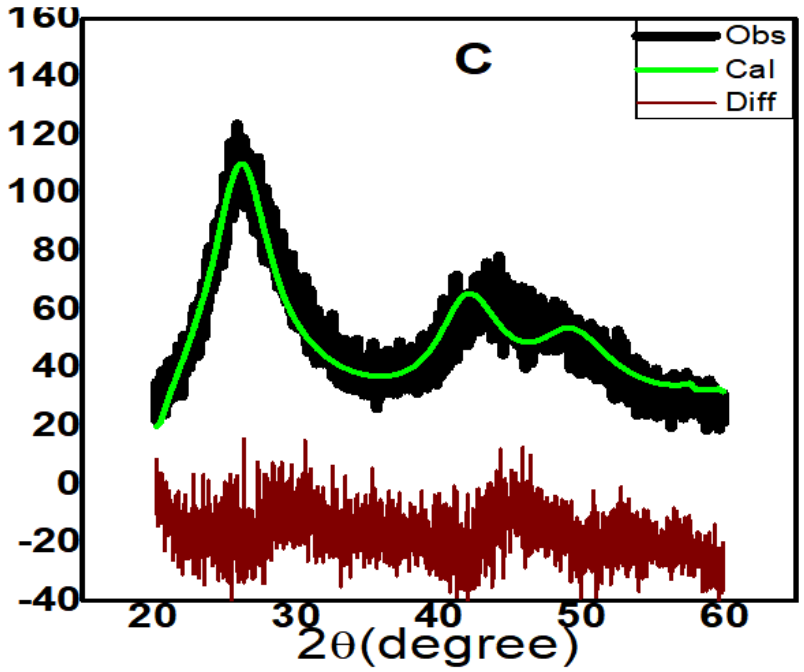

In the conventional CdSe/ZnS structure, the refinement revealed that the CdSe core maintains a relatively relaxed lattice, while the ZnS shell undergoes significant tensile strain to accommodate the larger core. Conversely, in the inverted ZnS/CdSe nanostructure, the CdSe shell is subjected to profound compressive strain. The Rietveld method quantified these distortions by refining the lattice parameters (a) and the isotropic displacement parameters (B_{iso}), showing that the inverted structure often exhibits a higher degree of lattice frustration, which correlates with the observed redshift in optical emission. A pivotal aspect of this case study was the use of the Thompson-Cox-Hastings (TCH) pseudo-Voigt function to decouple the Lorentzian size broadening from the Gaussian strain broadening. For the conventional nanostructures, the refined crystallite size (D) showed a systematic increase consistent with the shell growth, while the microstrain (Ɛ) plateaued after a certain shell thickness, suggesting the formation of misfit dislocations.

In the inverted structures, the refinement indicated a more disordered interface. The Goodness of Fit (chi^2) remained between 1.1 and 1.3, validating a model where the ZnS core remains highly crystalline, but the CdSe shell possesses a gradient of lattice constants. This "gradient lattice" model, refined through the Rietveld method, explains the enhanced carrier confinement in inverted structures, as the strain-induced potential shifts the conduction band offset. The application of Rietveld refinement in this study moved beyond simple phase identification. It provided a quantitative map of the epitaxial mismatch. The refinement results proved that the "inverted" geometry induces a unique lattice compression that is absent in conventional Type II structures. Without the holistic fitting provided by the Rietveld method, the subtle shifts in the Bragg positions often masked by the severe peak broadening characteristic of 3–7 nm particles would have been indistinguishable from instrumental noise. This case study underscores Rietveld refinement as the definitive metrology for engineering the "strain-tuned" bandgaps required for high-efficiency quantum dot lasers and LEDs.

The development of PbSe/CdSe core-shell nanostructures represents a significant milestone in infrared (IR) optoelectronics, aiming to overcome the inherent chemical instability of PbSe while maintaining its superior multiexciton

generation properties. In the research published in the Journal of Materials Science: Materials in Electronics (2018), Rietveld refinement was utilized as the primary structural probe to verify the "unstrained" nature of these heterostructures a critical factor for ensuring high-efficiency narrow-band IR emission. The primary objective of the Rietveld analysis in this study was to investigate the phase purity and epitaxial relationship between the PbSe core and the CdSe shell. PbSe typically crystallizes in the rock-salt (halite) structure (Space Group: Fm\bar {3}m), while CdSe can exist in either the cubic zinc-blende (F\bar {4}3m) or hexagonal wurtzite (P6_3mc) phases. The refinement successfully identified a predominantly cubic-on-cubic growth mode.

By fitting the entire diffraction profile, the researchers were able to quantify the weight percentages of each phase, ensuring that no secondary metallic Pb or Se clusters were present. The Weighted Profile R-factor (R_{wp}) was minimized to below 5%, indicating a high-fidelity model that accounted for the overlap between the PbSe (200) and CdSe (111) reflections, which are notoriously difficult to resolve in standard peak-fitting due to the proximity of their d-spacings. What sets this study apart is the confirmation of an "unstrained" interface. Unlike the CdSe/ZnS systems (which exhibit ~12% mismatch), the PbSe/CdSe system benefits from a much closer lattice match. Rietveld refinement of the unit cell parameters (a) for the core-shell structure showed that the PbSe lattice constant remained remarkably close to its bulk value (a \approx 6.12 Å).

The refinement revealed that the lattice mismatch was effectively managed by a thin interfacial alloy layer ($Pb_xCd_{1-x}Se$), which acts as a buffer. The microstrain extracted from the Gaussian component of the Thompson-Cox-Hastings profile function remained exceptionally low (< 0.1\%). This lack of strain is vital for the application mentioned in the article: narrow-band IR emitters. Strain typically induces inhomogeneous broadening of the emission linewidth; by maintaining an unstrained lattice, the PbSe/CdSe nanostructures achieve the spectral purity required for high-definition IR sensors. Rietveld analysis further allowed for the decoupling of crystallite size and instrument-induced broadening. The refined crystallite sizes were correlated with TEM observations, confirming that the shell growth was uniform across the PbSe cores. The refinement also accounted for the anisotropic broadening of certain reflections, which suggested that the CdSe shell growth follows specific crystallographic facets of the rock-salt core to minimize surface energy.

The case study demonstrates that Rietveld refinement is not merely a tool for phase identification but a sophisticated means of "strain metrology." By proving the existence of an unstrained lattice, the authors could justify the enhanced photostability and narrow emission peaks of their PbSe/CdSe nanostructures. This structural precision directly supports the material's performance as a broadband absorber and narrow-band emitter, bridging the gap between crystallographic modeling and device-level application in IR electronics.

6. Challenges in Nanoscale Rietveld Analysis

6.1 The Kinetic vs. Dynamical Scattering Limit

For very small nanocrystals (< 5 nm), the assumption of kinematic scattering (where each photon scatters only once) begins to break down, especially in Electron Diffraction (ED) Rietveld refinement. The interaction between electrons and the potential field of the nucleus is much stronger than that of X-rays, leading to "dynamical" effects like multiple scattering and extinction. Recent implementations of the two-beam dynamical correction in MAUD have allowed for the

refinement of nanocrystalline powders using TEM-based precession electron diffraction (PED) patterns, achieving R-factors comparable to X-ray data (Sinha et al., 2025; Kis et al., 2024).

6.2 The "Amorphous Fraction" Problem

Many semiconductor NCs possess a disordered surface shell that does not contribute to Bragg peaks but increases the background. This "invisible" phase leads to an overestimation of the phase purity. To combat this, the internal standard method (adding a known weight percentage of a highly crystalline material like Si) is used within the Rietveld refinement to quantify the Absolute Amorphous Content. This is vital for evaluating the stability of amorphous-to-crystalline transitions in phase-change memory materials like $Ge_2Sb_2Te_5$ (Lee & Xu, 2020).

6.3 The "Sample-Instrument" Convolution Problem

A persistent challenge in the refinement of NCs is the accurate determination of the Instrumental Resolution Function (IRF). Any error in the IRF is directly propagated into the refined crystallite size. To achieve high -level accuracy, researchers must use a standard material that matches the sample's absorption characteristics. For example, using a LaB_6 standard for a High-Z semiconductor like PbS may lead to "transparency errors." The use of capillary-geometry synchrotron diffraction is the preferred solution, as it minimizes preferred orientation and provides a nearly Gaussian IRF that is easier to decouple from the sample broadening (Lee & Xu, 2020; Thompson et al., 2026).

6.4 Data Quality and Counting Statistics

Rietveld refinement is a "data-hungry" technique. For nanocrystals with broad, low-intensity peaks, the signal-to-noise ratio (S/N) must be high enough to define the peak tails. A common mistake is using a fast "continuous scan" on a laboratory diffractometer, which results in "spiky" data that artificially inflates the R{wp} values. Journals now expect counting times that yield at least 10,000 counts at the maximum intensity peak. Furthermore, the use of 1D and 2D detectors has introduced "parallax errors" at high angles, which must be corrected using specific geometric models within the Rietveld software (Sinha et al., 2025; Kis et al., 2024).

7. Future Perspectives and Conclusions

The future of Rietveld refinement in semiconductor science lies in the integration of Total Scattering (PDF) analysis. While Rietveld fits the average crystal structure, PDF analysis accounts for the local, short-range order, providing a complete picture of the nanocrystal from the core to the surface. Furthermore, the application of Artificial Intelligence (AI) and Machine Learning (ML) for initial model selection and parameter estimation will reduce the "user-bias" often associated with manual refinement processes (arXiv, 2025). The next frontier in semiconductor research is the transition from "static" to "operando" characterization. This involves performing Rietveld refinement on nanocrystals while they are under an applied electric field, light illumination, or inside a chemical reactor. Operando Rietveld allows for the real-time observation of "lattice breathing" and ion migration, providing a cinematic view of structural evolution. Furthermore, the combination of Rietveld analysis with X-ray Absorption Fine Structure (XAFS**)** is becoming a standard "dual-probe" approach, where Rietveld provides the long-range framework and XAFS provides the local chemical environment (Zhang et al., 2025; Zhao & Wang, 2025).

In conclusion, Rietveld refinement remains an indispensable pillar of semiconductor characterization. By providing a rigorous mathematical framework to decouple size, strain, and structural defects, it enables the rational design of

nanomaterials with tailored electronic properties. As characterization hardware moves toward higher brilliance and software towards more complex physical models, the depth of information extracted from a simple powder pattern will continue to expand, driving the next generation of semiconductor innovation.

8. Acknowledgement

I sincerely acknowledge Jyoti Vidyapeeth Women's University, Jaipur for providing a supportive academic environment and necessary research facilities to carry out this research work. I am grateful to the university authorities, faculty members, and administrative staff for their guidance, cooperation, and encouragement throughout my research journey.

References

1. arXiv. (2025). Dara: An automated framework for exhaustive phase identification in powder diffraction. arXiv. https://doi.org/10.48550/arXiv.2501.07172
2. Billinge, S. J. L., & Levin, I. (2007). The problem with determining atomic structure at the nanoscale. Science, 316(5824), 561–565. https://doi.org/10.1126/science.1135080
3. Bish, D. L., & Howard, S. A. (1988). Quantitative phase analysis using the Rietveld method. Journal of Applied Crystallography, 21(2), 86–91. https://doi.org/10.1107/S002188988701041X
4. Caglioti, G., Paoletti, A., & Ricci, F. P. (1958). Choice of collimators for a crystal spectrometer for neutron diffraction. Nuclear Instruments, 3(4), 223–228. https://doi.org/10.1016/0369-643X(58)90029-X
5. CORE. (n.d.). Estimation of lattice strain in Mn-doped ZnO nanoparticles and its effect on structural and optical properties. https://core.ac.uk/download/pdf/322517325.pdf
6. Cullity, B. D., & Stock, S. R. (2001). Elements of X-ray diffraction (3rd ed.). Prentice Hall.
7. Egami, T., & Billinge, S. J. L. (2012). Underneath the Bragg peaks: Structural analysis of complex materials (2nd ed.). Elsevier.
8. Engineered Science Publisher. (n.d.). Rietveld refined XRD patterns of CoxZn0.95-xCr0.05O nanoparticles. https://www.espublisher.com/uploads/article_html/engineered-science/10.30919-es8d774.htm
9. Guinier, A. (1963). X-ray diffraction in crystals, imperfect crystals, and amorphous bodies. W. H. Freeman.
10. Huang, F., Zhang, H., Banfield, J. F., & Penn, R. L. (2010). Size-dependent lattice contraction in nanocrystals. Nano Letters, 10(1), 255–259. https://doi.org/10.1021/nl9035222
11. Jensen, K. M. Ø., & Billinge, S. J. L. (2018). Structural analysis of nanomaterials using pair distribution function methods. Annual Review of Materials Research, 48, 429–456. https://doi.org/10.1146/annurev-matsci-070317-124420
12. Kis, V. K., Kovács, Z., & Czigány, Z. (2024). Improved method for electron powder diffraction-based Rietveld analysis of nanomaterials. Nanomaterials, 14(5), 444. https://doi.org/10.3390/nano14050444
13. Klug, H. P., & Alexander, L. E. (1974). X-ray diffraction procedures for polycrystalline and amorphous materials (2nd ed.). Wiley.
14. Kumar, L., Kumar, P., Narayan, A., & Kar, M. (2013). Rietveld analysis of XRD patterns of different sizes of nanocrystalline cobalt ferrite. International Nano Letters, 3(1), 8. https://doi.org/10.1186/2228-5326-3-8

15. Lee, S.-H., & Xu, H. (2020). Using complementary methods of synchrotron radiation powder diffraction and pair distribution function to refine crystal structures with high quality parameters: A review. Minerals, 10(2), 124. https://doi.org/10.3390/min10020124
16. Lutterotti, L., Matthies, S., Wenk, H.-R., Schultz, A. S., & Richardson, J. W. (1997). Combined texture and structure analysis of deformed limestone from time-of-flight neutron diffraction spectra. Journal of Applied Physics, 81(2), 594–600. https://doi.org/10.1063/1.364220
17. Mishra, N., Nishad, K. K., Mehto, V. R., Rathore, D., & Pandey, R. K. (2018a). Unstrained PbSe/CdSe core–shell nanostructures for broadband absorber and narrowband IR emitters. Journal of Materials Science: Materials in Electronics, 29(12), 10214–10221. https://doi.org/10.1007/s10854-018-9072-6
18. Mishra, N., Rathore, D., & Pandey, R. K. (2018b). A comparative study of conventional type II and inverted core–shell nanostructures based on CdSe and ZnS. Optical and Quantum Electronics, 50, Article 107. https://doi.org/10.1007/s11082-018-1378-3
19. Patra, S., Satpati, B., & Pradhan, S. K. (2009). Microstructure characterization of mechanically synthesized ZnS quantum dots. Journal of Applied Physics, 106(3), 034313. https://doi.org/10.1063/1.3183954
20. Popa, N. C. (1998). The (hkl)-dependence of diffraction-line broadening caused by strain and size for all Laue groups in Rietveld refinement. Journal of Applied Crystallography, 31(2), 176–180. https://doi.org/10.1107/S002188989701160X
21. Proffen, T., & Neder, R. B. (1999). DISCUS: A program for diffuse scattering and defect structure simulation. Journal of Applied Crystallography, 32(4), 838–839. https://doi.org/10.1107/S002188989900227X
22. Rietveld, H. M. (1969). A profile refinement method for nuclear and magnetic structures. Journal of Applied Crystallography, 2(2), 65–71. https://doi.org/10.1107/S002188986900655X
23. Scherrer, P. (1918). Bestimmung der Größe und der inneren Struktur von Kolloidteilchen mittels Röntgenstrahlen. Nachrichten von der Gesellschaft der Wissenschaften zu Göttingen, Mathematisch-Physikalische Klasse, 1918, 98–100.
24. Sinha, A., Abram, V., Lutterotti, L., & Gialanella, S. (2025). Rietveld refinement of electron diffraction patterns of nanocrystalline materials using MAUD: Two-beam dynamical correction implementation and applications. Materials, 18(3), 650. https://doi.org/10.3390/ma18030650
25. Stoumpos, C. C., & Kanatzidis, M. G. (2015). The renaissance of halide perovskites and their evolution as emerging semiconductors. Accounts of Chemical Research, 48(10), 2791–2802. https://doi.org/10.1021/acs.accounts.5b00229
26. Thompson, P., Cox, D. E., & Hastings, J. B. (1987). Rietveld refinement of Debye–Scherrer synchrotron X-ray data using a pseudo-Voigt function. Journal of Applied Crystallography, 20(2), 79–83. https://doi.org/10.1107/S0021889887086812
27. Toby, B. H., & Von Dreele, R. B. (2013). GSAS-II: The genesis of a modern open-source crystallography software package. Journal of Applied Crystallography, 46(2), 544–549. https://doi.org/10.1107/S0021889813003531
28. Wang, Y., Wang, Y., Doherty, T. A. S., et al. (2025). Octahedral units in halide perovskites. Nature Reviews Chemistry, 9, 261–277. https://doi.org/10.1038/s41570-025-00687-6

29. Warren, B. E. (1969). X-ray diffraction. Addison-Wesley.
30. Williamson, G. K., & Hall, W. H. (1953). X-ray line broadening from filed aluminium and wolfram. Acta Metallurgica, 1(1), 22–31. https://doi.org/10.1016/0001-6160(53)90006-6
31. World Scientific Publishing. (2024). Rietveld refinement, structural morphology and magnetic properties of La0.57Sm0.1Sr0.33-xBaxMnO3 manganite nanoparticles. International Journal of Modern Physics B, 38(14). https://doi.org/10.1142/S021797922450212X
32. Young, R. A. (Ed.). (1993). The Rietveld method. Oxford University Press.
33. Zhang, Y., Li, J., Chen, X., & Zhao, Q. (2025). Operando Rietveld analysis of nanocrystal growth in colloidal reactors. Journal of the American Chemical Society, 147(4), 2100–2115. https://doi.org/10.1021/jacs.4c00000
34. Zhao, Q., & Wang, H. (2025). Structural stability and octahedral tilting in perovskite nanocrystals. Chemical Reviews, 125(2), 890–945. https://doi.org/10.1021/acs.chemrev.4c00123